Smart Structures and Systems, *Vol. 23, No. 1 (2019) 61-69*
DOI: https://doi.org/10.12989/sss.2019.23.1.061

Quasi real-time and continuous non-stationary strain estimation in bottom-fixed offshore structures by multimetric data fusion

Rajendra P. Palanisamy[1a], Byung-Jin Jung[2,3b], Sung-Han Sim[4c] and Jin-Hak Yi*[2,3]

[1]*Department of Civil and Environmental Engineering, Michigan State University, USA*
[2]*Ocean Science and Technology School, Korea Maritime and Ocean University, Republic of Korea*
[3]*Coastal Development Research Center, Korea Institute of Ocean Science and Technology, Busan, Republic of Korea*
[4]*School of Urban and Environmental Engineering, Ulsan National Institute of Science and Technology (UNIST), Republic of Korea*

(Received June 25, 2018, Revised January 11, 2019, Accepted January 13, 2019)

Abstract. Offshore structures are generally exposed to harsh environments such as strong tidal currents and wind loadings. Monitoring the structural soundness and integrity of offshore structures is crucial to prevent catastrophic collapses and to prolong their lifetime; however, it is intrinsically challenging because of the difficulties in accessing the critical structural members that are located under water for installing and repairing sensors and data acquisition systems. Virtual sensing technologies have the potential to alleviate such difficulties by estimating the unmeasured structural responses at the desired locations using other measured responses. Despite the usefulness of virtual sensing, its performance and applicability to the structural health monitoring of offshore structures have not been fully studied to date. This study investigates the use of virtual sensing of offshore structures. A Kalman filter based virtual sensing algorithm is developed to estimate responses at the location of interest. Further, this algorithm performs a multi-sensor data fusion to improve the estimation accuracy under non-stationary tidal loading. Numerical analysis and laboratory experiments are conducted to verify the performance of the virtual sensing strategy using a bottom-fixed offshore structural model. Numerical and experimental results show that the unmeasured responses can be reasonably recovered from the measured responses.

Keywords: strain estimation; multimetric data fusion; Kalman filter; buffer; nonstationary responses; offshore structures

1. Introduction

Bottom-fixed offshore structures such as monopiles, tripods, jackets, and gravity-based structures have been widely utilized for the purpose of extracting oil and gas and supporting metrological towers and multipurpose ocean science platforms, and their applications are expanded for supporting ocean energy facilities (OEFs) including offshore wind turbines and tidal stream turbines. Indeed, in recent years, the number of bottom-fixed offshore structures has been increasing rapidly with the increase in the large-scale offshore wind farms (EWEA 2015). Because these offshore structures are generally built in harsh environments, strong winds and tidal currents can cause structural degradation (fatigue and corrosion) that leads to catastrophic failure. In addition, the quasi-periodic excitation forces due to the rotating devices including rotors, main shafts, and generators can be a source of fatigue (BMT report 2013, Ren and Zhou 2014, Yeter *et al.* 2015). Being prone to the structural failures due to various external excitations, these offshore structures for OEFs are carefully maintained to prevent catastrophic collapses and to prolong their lifetime.

Structural health monitoring (SHM) provides an effective means of maintaining the offshore structures appropriately to assess the present status as well as the remaining lifetime. SHM is typically performed by collecting the response data measured from a limited number of accessible locations using sensors such as accelerometers and strain gauges. In the monitoring of the offshore structures of OEFs, most of the fatigue-sensitive spots and critical members are located in regions that are inaccessible for direct measurements (e.g., at the mudline several ten meters below the water level). Thus, the sensor installation at important regions deep inside the water can be quite challenging.

Recently, virtual sensing approaches are being actively developed for offshore wind turbines to indirectly obtain the responses at the unmeasured locations by using the measured responses such as acceleration and strain (Paust 2015, Iliopoulos *et al.* 2015, Ren and Zhou 2014). The virtual sensing technologies can be classified as data-driven techniques, such as the neural network-based methods, and model-driven techniques, such as Kalman filtering (Kalman 1960) with finite element (FE) models.

The model-based virtual sensing technology has been intensively studied for estimating the unmeasured responses from a limited set of response data based on the Kalman filter (Van der Male and Lourens 2014, Papadimitriou *et al.* 2010, Park *et al.* 2013, Park *et al*. 2014, Cho *et al.* 2014,

*Corresponding author, Ph.D. Principal researcher, Professor
E-mail: yijh@kiost.ac.kr
[a] Ph.D. Student
[b] MS Student
[c] Ph.D., Associate Professor

Copyright © 2019 Techno-Press, Ltd.
 ISSN: 1738-1584 (Print), 1738-1991 (Online)

and Jo and Spencer 2014) and modal decomposition and expansion (Iliopoulos *et al*. 2014). Joint input-response estimation techniques are developed to improve the accuracy of estimation (Lijun *et al*. 2016, Maes *et al*. 2015, Lourens *et al.* 2012). Iliopoulos *et al*. (2014) proposed response estimation techniques using a modal decomposition and expansion algorithm and validated the performance of their method using the measurement data obtained from a monitoring campaign on an offshore Vestas V90 3 MW wind turbine mounted on a monopile foundation. Further, similar algorithms with data fusion techniques are used in reference-free displacement estimation (Cho *et al.* 2016) and the estimation of a flexibility matrix (Sim 2016). Van der Male and Lourens (2014) proposed a strategy to monitor the accumulated fatigue damage in real time by employing a joint input-state estimation algorithm. Measuring the operational vibrations at appropriate locations enables the estimation of strain responses at the unmeasured locations. The estimation algorithm is applied to a wind turbine mounted on a lattice support structure for which the response estimates of the lattice members are based on the measurements obtained only from the turbine tower. Most of these studies are limited to zero mean responses, and their algorithm is verified only using numerically simulated responses. Some recent experimental results have been reported by Maes *et al.* (2016) and Iliopoulos *et al*. (2017).

This study investigates a near real-time virtual sensing strategy based on Kalman filtering associated with an FE model tailored to the offshore structures under non-zero mean stochastic external loads. A multimetric data fusion technique is incorporated to overcome the difficulties related to the non-zero mean static response estimation. This technique is implemented by the fusion of different sensors such as strain gauges and accelerometers for low and high-frequency regions. The bottom-fixed offshore structures of OEFs consists of broad spectrum of strain responses because of the thrust force as well as the dynamic excitations due to the turbulent effect and the periodic operational loads due to the rotors. Therefore, extracting accurate responses from homogeneous sensor networks using either acceleration or strain is quite challenging. Thus, a multi-sensor network is more appropriate to estimate broad spectrum responses.

The proposed method includes a buffering technique, which reduces the computation time significantly in contrast to any other estimation techniques. Thus, this estimation technique can be easily implemented in wireless and mobile sensing technologies (Lee and Kim 2016). The proposed method is verified numerically and experimentally using a four-legged portal frame in a circulating water channel.

2. Formulation

Monitoring the offshore structures under water is unique in that the sensor installation and maintenance associated with the data acquisition systems are quite challenging because critical structural members are often inaccessible.

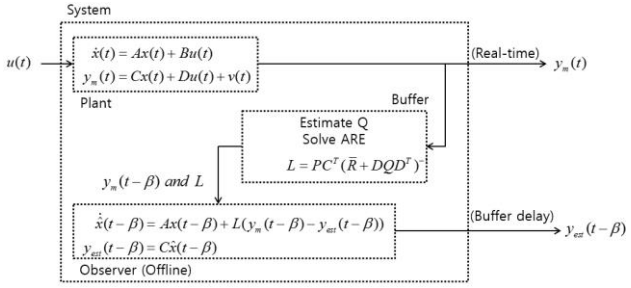

Fig. 1 Kalman state observer with buffer

Furthermore, strong tidal currents, debris and installation error could cause sensor malfunctioning. Estimating structural responses at the important unmeasured locations can be a powerful alternative to the direct measurement when the direct measurement is not available. Despite the usefulness of the response estimation technique, it has not been fully explored in the literature yet. This study investigates the Kalman filter-based data fusion technique to estimate the unmeasured non-stationary strain data from an offshore structure, which can be subsequently used to assess structural conditions such as the fatigue remaining life of steel members in the offshore structure. As this study focuses on monitoring the offshore structures, we consider two major aspects that need to be addressed appropriately:

1) Offshore structures are continuously subjected to non-zero mean input excitations because of tidal currents.

2) Sensors are prone to damage because of the harsh environments or are difficult to install and manage in some hot spots.

The input forces, as well as the structural responses, have a large amplitude trend that varies slowly according to the changing speed and direction of the tidal current. Thus, the response estimation algorithm should be capable of handling non-zero mean inputs. Further, sensor malfunction and inaccessibility of some hot spots in offshore structures demand the algorithm to estimate complete responses with limited measurements (Palanisamy *et al.* 2015).

A buffering technique is added to the conventional Kalman filter algorithm for near real-time responses estimation in structures that are subjected to non-stationary random loading. The Kalman filter provides an efficient computational means to estimate the state of a process in a way that minimizes the mean of the squared error (Crassidis and Junkins 2012). The buffering technique pre-processes a segment of measured responses that strategically enables Kalman filter to work under non-stationary loading.

2.1 System design

The general Kalman filter-based state estimator requires a known input. Further, it assumes that the state disturbances and the sensor noise are stationary. In reality, offshore structures are subjected to unknown non-stationary random inputs. Thus, a buffering technique is added to the general Kalman filter that strategically performs the response estimation under unknown non-stationary random inputs. The simplified block diagram of the state estimator is shown in Fig. 1. The state estimator has three major parts:

a plant, a buffer, and an observer. In this study, the plant is the actual structure, which is intractable, and the observer can be designed depending on the output of interest. The buffer is an addition to the typical Kalman estimator. This technique enables the estimator to handle non-stationary inputs in real time with a buffer delay.

2.1.1 Plant

The equation of motion of the considered linear system or plant is given as follows

$$M\ddot{x}(t)+C\dot{x}(t)+Kx(t)=u(t) \tag{1}$$

where $x(t)$, $\dot{x}(t)$, and $\ddot{x}(t)$ are the displacement, velocity and acceleration, respectively, and M, C, and K are the mass, damping, and stiffness matrices of the dynamic system, respectively. $u(t)$ is the input force vector applied to the system. Eqs. (2) and (3) express the state-space model of the system.

$$\dot{x}(t)=Ax(t)+Bu(t) \tag{2}$$

$$y_m(t)=Cx(t)+Du(t)+v(t) \tag{3}$$

where matrices C and D in Eq. (3) are selected depending on the output of interest $y_m(t)$; input $u(t)$ and measurement noises $v(t)$ possess a covariance $Q(t)=E\left[u(t)u(t)^T\right]$ and $R(t)=E\left[v(t)v(t)^T\right]$, respectively. Matrices A and B are system matrices.

2.1.2 Observer design

As the input force vector, $u(t)$, is unknown, the typical Kalman estimator is slightly modified for near real-time application without the input, $u(t)$. Eqs. (4) and (5) indicate the observer design.

$$\dot{\hat{x}}(t-\beta)=A\hat{x}(t-\beta)+L(y_m(t-\beta)-y_{est}(t-\beta)) \tag{4}$$

$$y_{est}(t-\beta)=C\hat{x}(t-\beta) \tag{3}$$

where β is the buffer time, $\hat{x}$ is the estimated state, and L is the Kalman gain, which is selected to minimize the steady-state error covariance. y_{est} is the estimated output.

2.1.3 Buffer

This section explains how the buffer prepares the data and the Kalman gain for the observer to handle a non-stationary random input. The error dynamics of the complete system (plant + observer) without the buffer in real time is derived as

$$\dot{e}(t)=(A-LC)e(t)+Bu(t)-L(Du(t)+v(t)) \tag{6}$$

where e is the difference between the actual state and the estimated state, $e=x-\hat{x}$. The objective of the Kalman filter is to minimize the covariance of e.

$$P(t)=E[e(t)\,e(t)^T] \tag{7}$$

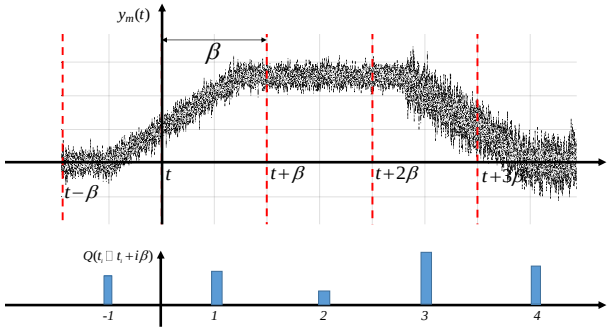

Fig. 2 Input covariance estimation from time segments of preloaded measurement data

The rate of change of error covariance is given as

$$\begin{aligned}\dot{P}(t)&=(A-LC)P(t)+P(t)(A-LC)^T\\&+BQ(t)B-P(t)C^T\bar{R}(t)^{-1}CP(t)\end{aligned} \tag{8}$$

To minimize error covariance $P(t)$. $\dot{P}(t)$ is equated to zero and solved using an algebraic Riccati equation. It is necessary that $Q(t)$, $R(t)$, and $P(t)$ in Eq. (8) should be time invariant to equate $\dot{P}(t)$ to zero. However, in the considered case, input covariance $Q(t)$ is non-stationary, i.e., the statistical properties of the input changes over time. In order to solve this issue, a buffering technique is introduced (see Fig. 1) where the measured data are preloaded and processed to estimate an input covariance during Q the complete time segment, β, (See Fig. 2). The equation of input covariance after introducing the buffering technique is given as

$$Q^S=E\left[(u^S)(u^S)^T\right] \tag{9}$$

where, Q^S is the input covariance between time t and $t+\beta$. u^S is the input between time t and $t+\beta$. As we have the complete knowledge of Q for the time segment β, we can safely assume that the input covariance is bounded and time invariant within the selected time segment β. Thus, $\dot{P}(t)$ in Eq. (8) can be equated to zero, and it takes the form of a continuous-time algebraic Riccati equation (CARE).

$$0=(A-LC)P+P(A-LC)^T+BQB-PC^T\bar{R}^{-1}CP \tag{10}$$

where $\bar{R}=(DQD+R)$ and the solution, P, from CARE is used to build the Kalman gain, L.

$$L=PC^T\left(\bar{R}+DQD^T\right)^{-1} \tag{11}$$

The value of L behaves optimally within the time segment β. This enables the observer to handle the non-stationary input. It is important to note that Eqs. (10) and (11) should be recalculated for every time segment β. Further, while the observer is working on the offline data from the buffer, the buffer will load the data corresponding

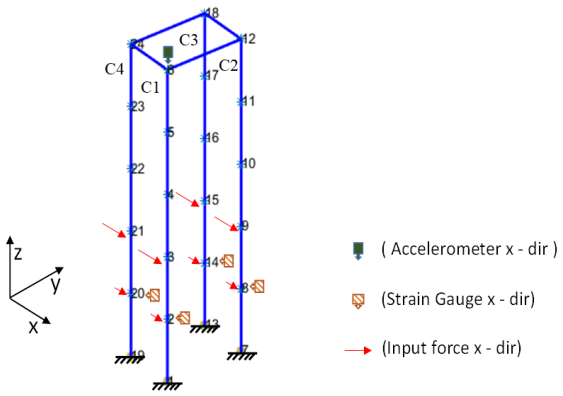

Fig. 3 Numerical model

to the next time segment and estimate Q^S. Thus, the overall system estimates the response in real time with a buffering time delay of β (subjected to the hardware used for computation). The buffer duration shall be decided on the knowledge of loading history. These modifications in the filter are verified numerically and experimentally as described in the following sections.

3. Numerical validation

This section presents a numerical model of an offshore structure (see Fig. 3). To simulate the tidal current loading, this model is simulated using MATLAB Simulink under non-zero mean input excitation. A limited number of responses is collected and used in the Kalman filter-based response estimation algorithm to obtain the unmeasured responses.

3.1 Simulation setup

The model is composed of 24 frame elements, each of which has a length of 0.2 m as shown in Fig. 3. The columns (C1, C2, C3, and C4) have the same circular cross section of radius 3 cm. It is assumed that the columns and the top plate are made of high-density polyethylene (HDPE) and steel, respectively. The Young's modulus and the mass density of the columns presented here are 1,000 MPa and 953 kg/m^3, respectively. The Young's modulus and density of the four frame members on the top of the columns are 210 GPa and 7,850 kg/m^3, respectively. The developed numerical model is used in MATLAB Simulink to simulate the acceleration and strain responses under the non-zero mean inputs that are applied to the first two nodes of each column as shown in Fig. 3. Although all four columns are forced under a single stream, they may not have a similar stream velocity. The turbulence, stream direction, and structure complexity will change the stream velocity in each column, which in turn will change the input force at each column. However, the input forces are dependent on the speed and direction of the mainstream. Thus, for simulation, columns 1 and 2 in the downstream are assumed to experience a force 50% less than columns 3 and 4 in the upstream velocity (based on experimental experience). Responses are sampled at 150 Hz. The acceleration data is numerically contaminated by 2% noise in the root mean square (RMS), whereas the strain is contaminated by 10% noise in the RMS based on the experience of higher noise on the actual strain measurement (Palanisamy *et al*. 2015). These limited responses are used to predict the input covariance and the unmeasured responses.

3.1.1 Input covariance estimation

From the simulation setup, it can be understood that the input forces on each column are different but they are not independent. Using this idea, we calculated a strain relationship matrix as shown in Eq. (12). This matrix is calculated when all the sensors are active. The Kalman state estimator estimates the input covariance Q^S in its buffer part using the available measurement y_m^S. There are two steps involved in estimating the input covariance. In Step 1, the missing strain data is estimated using the available strain data and strain relationship matrix (see Eq. (13)). The estimated strain may not be accurate; the only purpose of this estimation is to estimate the input covariance in the next step. In Step 2, with the help of the numerical model, a flexibility matrix K_{sp} is constructed using strain ε^s and input force u^s as shown in Eq. (14). With this relation, the measured strain responses can be transformed to the input forces.

$$\varepsilon\varepsilon = \begin{bmatrix} \left\{\frac{std(\varepsilon_i)}{std(\varepsilon_j)}\right\} & \left\{\frac{std(\varepsilon_i)}{std(\varepsilon_j)}\right\} & \mathrm{K} \\ \left\{\frac{std(\varepsilon_i)}{std(\varepsilon_j)}\right\} & \left\{\frac{std(\varepsilon_i)}{std(\varepsilon_j)}\right\} & \mathrm{K} \\ \mathrm{M} & \mathrm{M} & \mathrm{O} \end{bmatrix} \tag{12}$$

$$\varepsilon^S = \varepsilon\varepsilon y_m^S \tag{13}$$

$$u^S = K_{sp}\varepsilon^S \tag{14}$$

The accuracy of the estimated input, u^S, depends on the accuracy of the FE model used. However, the observer gain, L, depends only on the covariance of input Q^S as shown in Eq. (11), which does not require an accurate FE model.

3.1.2 Multimetric data fusion

Further, to improve the accuracy of estimation, the multimetric data fusion technique is adopted. The acceleration and strain responses are chosen for data fusion. Unlike the accelerometer, strain gauges are sensitive to the electrical noise and local defects in a structure. Acceleration being a poor low-frequency observer, the quasi-static trend of non-zero mean responses is generally difficult to capture in comparison to the strain gauges. Thus, the fusion of the multimetric data (strain and acceleration) will enhance the accuracy of the response estimation (Park *et al*. 2013, Park *et al*. 2014, Cho *et al*. 2014, Jo and Spencer 2014).

Table 1 Measured and estimated response for each case

Case	Measured strain location	Measured acceleration location	Estimated strain location
1	8, 14, and 20	6	2
2	2, 14, and 20	6	8
3	2, 8, and 20	6	14
4	2, 8, and 14	6	20

Four different simulation cases are considered here. In each case, one of the strain responses is estimated with the help of other strain and acceleration responses (see Table. 1). For example, in case 1, the strain measurements near the root of columns 2, 3, and 4 and the acceleration at the top of the columns (see Fig. 3) are used to estimate the strain response of column 1.

3.2 Estimation result

Fig. 4 shows the estimated strain in each case. Each case is processed in two steps:

1) Step 1: estimate the input covariance, Q, and calculate the Kalman gain, L.
2) Step 2: use the Kalman gain, L, and the limited measurements in the Kalman filter-based state estimator to estimate the unmeasured responses.

In case 1, the strain response at nodes 8, 14, and 20 with the acceleration response at node 6 are used to estimate the strain at node 2. During the input covariance estimation, the strain response at unmeasured node 2 is replaced with that at node 8 because they experience a similar stress state. A similar procedure is followed to estimate the strain response at the other columns as shown in Table 1. From Fig. 4, the estimated non-zero mean strain at each column is in good agreement with the reference strain. Because of the large upstream force, columns 3 and 4 experience a higher strain compared to columns 1 and 2. Fig. 5 shows the capability of the algorithm to estimate the dynamic component of the response.

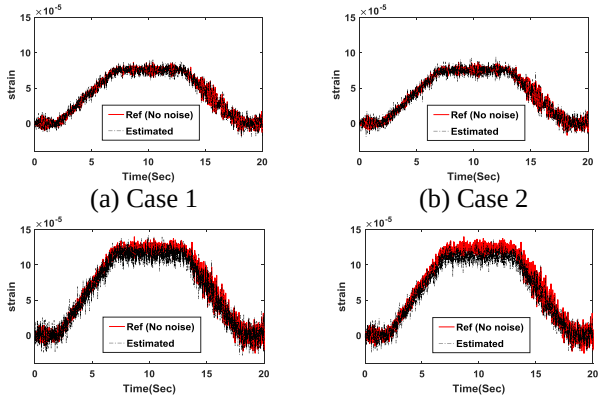

(a) Case 1 (b) Case 2

(c) Case 3 (d) Case 4

Fig. 4. Estimated and reference strain responses in time domain

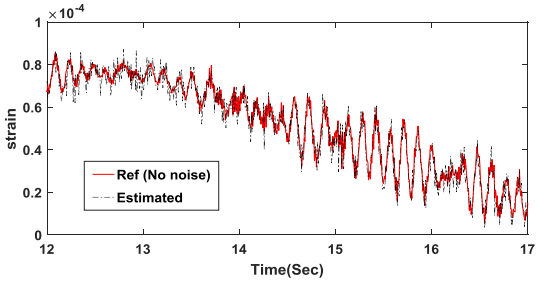

Fig. 5 Estimated and reference strain response in column 1 (between 12 s and 17 s)

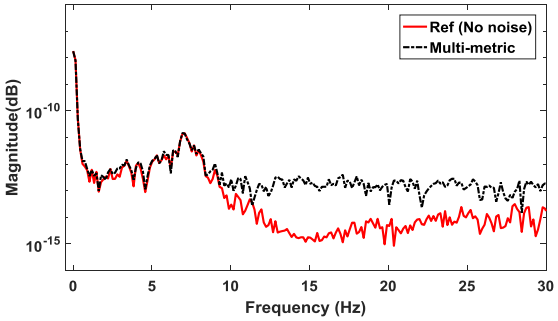

Fig. 6 Estimated and reference strain responses in frequency domain

In addition to the comparison in the time domain, the estimated and measured strain responses are compared in the frequency domain by plotting their power spectra as shown in Fig. 6. Note that only case 1 is shown as all the cases exhibit similar power spectra. From Fig. 6, it can be observed that the estimated strain is in good agreement with the reference strain. Their strong agreement near 0 Hz shows the capability of the algorithm to handle non-stationary responses.

To investigate the consistency of the response estimation, root mean square errors (RMSEs) between the reference and estimated strains were calculated as

$$Error = \frac{\sqrt{\sum\left(\varepsilon_{est} - \varepsilon_{ref}\right)^2}}{\sqrt{\sum\left(\varepsilon_{ref}\right)^2}} \tag{15}$$

where ε_{ref} is the reference strain and ε_{est} is the estimated strain. Fig. 7 shows the RMSEs calculated for each column. The error in the response estimation for each column is less than 2%. The estimation errors in columns 3 and 4 are relatively higher when compared to columns 1 and 2. Because columns 3 and 4 experience a larger upstream force (see Figs. 3 and 4), thus the estimation error is also higher. However the more quantitative error analysis is not covered in this study.

Further, the estimation error corresponding to a different level of observation noise in the strain and acceleration data is tested. Fig. 8 indicates that the estimation error increases with an increase in the measurement noise. A similar trend

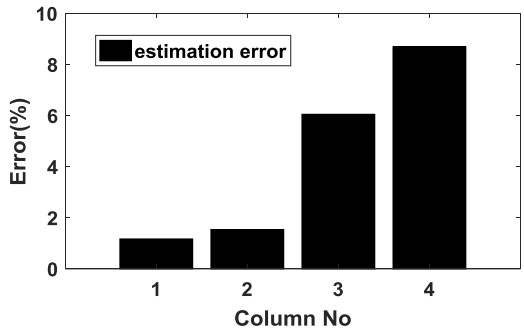

Fig. 7 Estimation errors

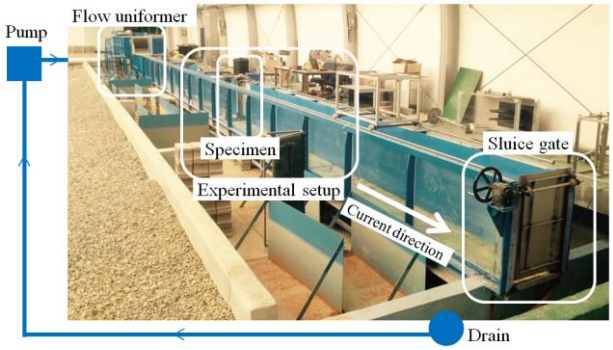

Fig. 9 Circulating water channel setup

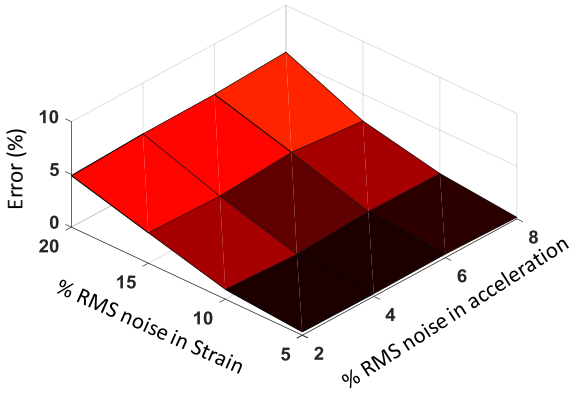

Fig. 8 Estimation error in column 1 for different observation noise

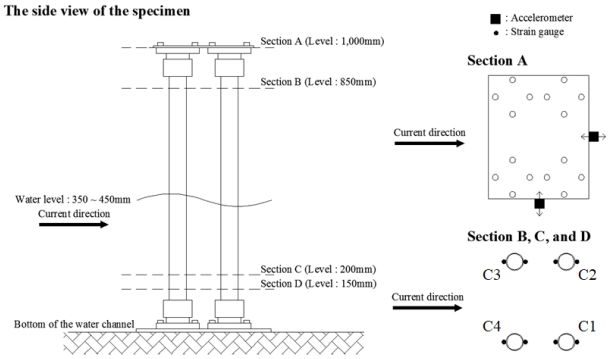

Fig. 10 Specimen with deployed strain gauge and accelerometer

is observed in all the columns; thus, only the results corresponding to column 1 are shown. From Fig. 8, it can be observed that the measurement noise in the strain has a larger influence on the estimation error when compared to the acceleration noise.

4. Experimental validation

This section describes the experimental validation of the response estimation approach using a scaled model of an offshore structure. The experiment is conducted in a flume with a controlled water current. The measured responses are used to validate the response estimation algorithm.

4.1 Experimental setup

The experiment is carried out in a circulating water channel as shown in Fig. 9. The length, width, and height of the circulating water channel are 24 m, 480 mm, and 900 mm, respectively. A specimen is installed 9 m away from the sluice gate to avoid the effect of the reflected water current from the gate and to ensure a uniform flow.

Fig. 10 shows the dimension of the specimen and the deployed sensors. Table 2 lists the material properties and the dimensions of the top plate and columns, which are the parts of the experimental specimen. The strain gauges are attached to each column at 150 mm from the root of the specimen. A waterproof material is applied to avoid the strain gauges from malfunctioning. A half-bridge configuration is used to improve the sensitivity of the strain gauges. The acceleration and strain responses are measured at a sampling rate of 200 Hz by the data acquisition devices (DAQ).

Fig. 11 shows the specimen with and without the water current. It can be observed that the upstream water level is higher than the downstream in the columns that experience more turbulence compared to the other columns. Thus, the columns in the upstream will experience a different force than that in the downstream.

Table 2 Material properties and dimension of experimental specimen

Properties	Top plate	Columns
Material	Steel	High-density polyethylene (HDPE)
Young's modulus	210 GPa	1,000 MPa
Shear modulus	79.3 GPa	800 MPa
Density	7,850 Kg/m^3	953 Kg/m^3
Size	430 mm x 350 mm x 9 mm	D60 mm x 5 mm height: 1000 mm
Weight	10.63 kg (without accessories)	0.823 kg/each column (without connector)

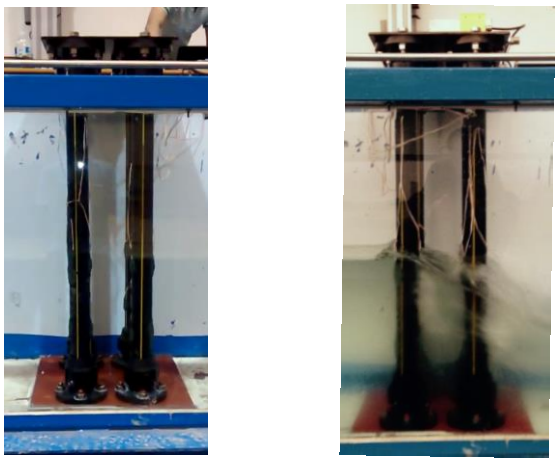

(a) without water current (b) with water current

Fig. 11 Specimen

The experiment is carried out in the following steps. Initially, the flume is filled to a water level of 400 mm by shutting the sluice gate at the end of the water channel (see Fig. 9). Next, the pump is turned on and the sluice gate is controlled to maintain the same water level throughout the experiment. After a few minutes, the pump is turned off and simultaneously the sluice gate is controlled to maintain the same water level.

4.2 Estimation results

Fig. 12 compares the experimental and estimated strain response of each column. The validation cases considered here are similar to the cases seen in the numerical validation. From the experimental strain response, it can be observed that during the first 60 s, the water is still, and after 60 s, the current velocity increases rapidly until 130 s. The water velocity is maintained constantly for about 100 s and gradually decreased to zero. The response estimation algorithm uses the same FE model used in the numerical validation. The estimation consists of two steps. Step 1: estimate the input time history of each column with limited responses (Eq. (12)); the strain at the unmeasured location is assumed the same as the nearest available strain response. Step 2: calculate the input covariance with the available input time history and use the limited response in the Kalman filter-based response estimation algorithm to estimate the unmeasured responses. The overall estimation shown in Fig. 12 is in good agreement with the measured responses. As it is difficult to observe the dynamic component of estimation from Figs. 12 and 13 shows the estimation between 240 s and 250 s. It is also notable that the strain levels for columns in upstream, i.e. Columns 3 and 4, are almost same to those for columns in downstream, and this is not consistent to the assumption in numerical simulation study. This might be because the current velocity is increased passing through the upstream columns and there is a certain level of blockage effect due to the narrow channel width.

Fig. 14 shows the frequency domain comparison between the measured and estimated responses. It can be observed that the estimation is in good agreement near 0 Hz, which clearly shows the ability of the algorithm to capture the quasi-static responses. The comparison results corresponding to each column exhibits similar power spectral responses. Thus, Fig. 14 shows only the result corresponding to column 1. Unlike the reference strain from the numerical model, the strain data from the experiment is subjected to small electrical noise (see Fig. 14). A 60 Hz peak can be observed from the figure.

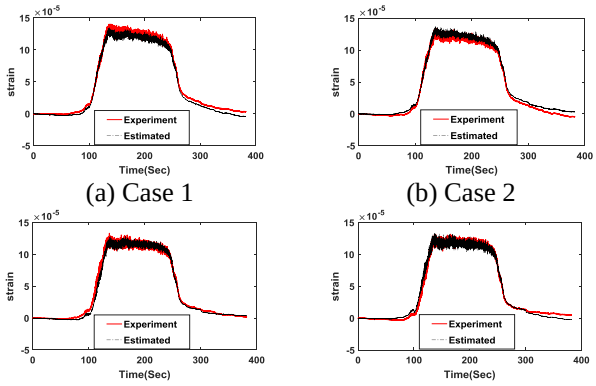

(a) Case 1 (b) Case 2

(c) Case 3 (d) Case 4

Fig. 12 Estimated and experimental strain responses in time domain

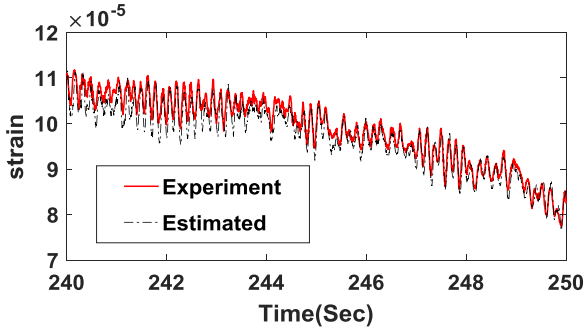

Fig. 13 Estimated and experimental strain responses in column 4 (between 240 s and 250 s)

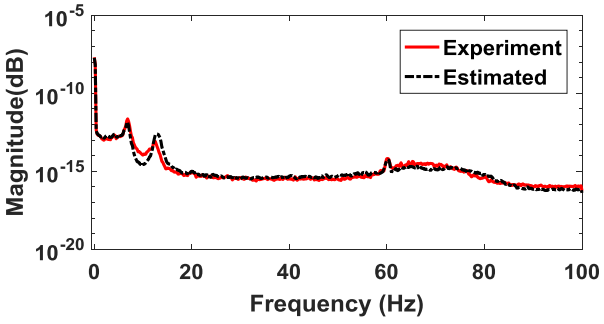

Fig. 14 Estimated and experimental strain responses in frequency domain

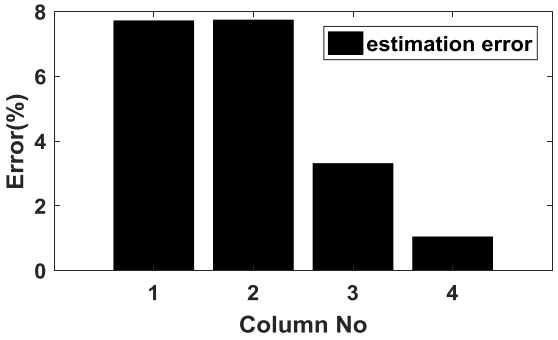

Fig. 15 Error in estimated strain at each column

Fig. 15 shows the RMSE in the strain estimated for each column. The strain estimation in columns 1 and 2 has a higher percentage of error. The strain gauges should be deployed perpendicular to the plane of bending else the measured responses may not be accurate. Because the model and the estimator are designed to work with strain measured purely along the x-direction, the higher errors in columns 1 and 2 could be due to improper sensor deployment. Columns 3 and 4 have an error of approximately 1-3%.

5. Conclusions

The virtual sensing strategy that is tailored to the SHM of offshore structures was investigated in this study. As the important structural members of offshore structures are located under water, the virtual sensing strategy can be a powerful alternative to the direct measurement, particularly when the structural responses are desired due to unavailable sensors. The problem formulation for the near real-time virtual sensing based on Kalman filtering was provided with how the non-stationary random excitation can be properly handled for accurate response estimation. Two different types of data, acceleration and strain, were input to the state estimator. The strain response contributes to the low frequency, large amplitude trend in the estimation, whereas the acceleration with a high-frequency information is capable of reducing the random noise. The numerical simulation was conducted with the FE model of a small-scale offshore structure. The non-stationary input excitation that varies with time and height is introduced to simulate the tidal current. The overall simulation result indicated that the estimation was accurate with errors between 1 - 10%. A laboratory experiment was conducted subsequently with the small-scale offshore structure installed in a water channel. The virtual sensing strategy successfully obtained a strain response using the other three strains and the acceleration of the top plate. The numerical analysis and the experiment lead to the following conclusions:

- The virtual sensing strategy has the potential to capture structural responses of the bottom-fixed offshore structures under the non-stationary tidal current.
- The combined use of the different types of measurements (i.e., strain and acceleration) can help improve the estimation of the unmeasured strain response in lower and higher frequency regions.

The virtual sensing strategy is observed to be quite useful for monitoring offshore structures. Based on the findings in this paper, further studies may use the estimated response for the SHM purposes such as fatigue estimation and damage detection.

Acknowledgements

This research was a part of the project titled "Development of active-controlled tidal stream generation technology" funded by the Ministry of Oceans and Fisheries, Korea (20110171) and KIOST R&D Program (project No. PE99731).

References

BMT Fleet Technology Ltd. (2013), *Fatigue design review of offshore wind turbine generator structures*, Final Report.

Cho S., Park, J.P., Palanisamy R.P. and Sim, S.H. (2016), "Reference-free displacement estimation of bridges using Kalman filter-based multimetric data fusion", *J. Sensors*, Article ID 3791856.

Cho S., Sim, S.H., Park, J.P. and Lee, J. (2014), "Extension of indirect displacement estimation method using acceleration and strain to various types of beam structures", *Smart Struct. Syst.*, **14** (4), 699-718.

Crassidis, J.L. and Junkins, J.L. (2012), *Optimal estimation of dynamic systems*. Second edition, CPC press, Taylor & Francis Group, ISBN -13: 978-1-4398-3986-7.

EWEA (2015), *Aiming high rewarding ambition in wind energy*. The European Wind Energy Association.

Iliopoulos, A.N., Devriendt, C., Guillaume, P. and Van Hemelrijck, D. (2014), "Continuous fatigue assessment of an offshore wind turbine using a limited number of vibration sensors", *Proceedings of the 7th European Workshop on Structural Health Monitoring*, July 8-11, 2014. La Cite, Nantes, France.

Iliopoulos, A.N., Weijtjens, W., Van Hemelrijck, D. and Devriendt, C. (2015), "Prediction of dynamic strains on a monopile offshore wind turbine using virtual sensors", *J. Phys.: Conference Series*, 628, 012108

Iliopoulos, A.N., Weijtjens, W., Van Hemelrijck, D. and Devriendt, C. (2017), "Fatigue assessment of offshore wind turbines on monopile foundations using multi-band modal expansion", *Wind Energy*, **20**(8), 1463-1479.

Jo, H. and Spencer, B.F. (2014), "Multimetric model based structure health monitoring", *Proceedings of the SPIE, Sensors and Smart Structures Technologies for Civil, Mechanical, and Aerospace Systems 2014*, San Diego, California, USA, March.

Kalman, R.E. (1960), "A new approach to linear filtering and prediction problem", *J. Basic Eng.*, **82**(1), 35-45.

Lee J.H. and Kim. S.C. (2016), "Mobile technology in the field data collection and management", *J. Struct. Integrity Maint.*, **1**(3), 140-145.

Liu, L., Zhu, J., Su, Y. and Lei, Y. (2016), "Improved Kalman filter with unknown inputs based on data fusion of partial acceleration and displacement measurements", *Smart Struct. Syst.*, **17**(6), 903-915.

Lourens, E., Papadimitriou, C., Gillijns, S., Reynders, E., DeRoeck, G. and Lombaert, G. (2012), "Joint input-response estimation for structural systems based on reduced-order models and vibration data from a limited number of sensors", *Mech.*

Syst. Signal Pr., **29**, 310-327.
Maes, K., Iliopoulos, A., Weijtjens, W., Devriendt, C. and Lombaert, G. (2016), "Dynamic strain estimation for fatigue assessment of an offshore monopile wind turbine using filtering and modal expansion algorithms", *Mech. Syst. Signal Pr.*, **76-77**, 592-611.
Maes, K., Smyth, A. W., De Roeck, G. and Lombaert, G. (2015), "Joint input-state estimation in structural dynamics", *Mech. Syst. Signal Pr.*, **70-71**, 445-466.
Palanisamy, R.P., Cho, S., Kim, H. and Sim, S.H. (2015), "Experimental validation of Kalman filter-based strain estimation in structures subjected to non-zero mean input", *Smart Struct. Syst.*, **15**(2), 489-503.
Papadimitriou, C., Fritzen, C.P., Kraemer, P. and Ntotsios, E. (2010), "Fatigue predictions in entire body of metallic structures from a limited number of vibration sensors using Kalman filtering", *Struct. Control Health Monit.*, **18**(5), 554-573.
Park, J.W., Sim, S.H. and Jung, H.J. (2013), "Displacement estimation using multimetric data fusion", *IEEE/ASME T. Mechatron*., **18**(6), 1675-1682.
Park, J.W., Sim, S.H. and Jung, H.J. (2014), "Wireless displacement sensing system for bridges using multi-sensor fusion", *Smart Mater. Struct.*, **23**(4).
Paust, H.S. (2015), *Finite element modeling and structural state estimation of a bottom fixed offshore wind turbine*, M.S. thesis, Norwegian University of Science and Technology.
Ren, P. and Zhou, Z. (2014), "Strain response estimation for the fatigue monitoring of an offshore truss structure", *Pacific Sci. Rev.*, **16**, 29-35.
Sim, S.H. (2016), "Estimation of flexibility matrix of beam structures using multisensor fusion", *J. Struct. Integrity Maint.*, **1**(2), 60-64.
Van der Male, P. and Lourens, E. (2014), "Operational vibration-based response estimation for offshore wind lattice structures", *Proceedings of the International Modal Analysis Conference.*
Yeter, B., Garbatov, Y. and Guedes Soares, C. (2015), "Fatigue damage assessment of fixed offshore wind turbine tripod support structures", *Eng. Struct.*, **101**, 518-528.

HJ